

Topological advantage for adsorbate chemisorption on conjugated chains

Luis Martinez-Gomez and Raphael F. Ribeiro*

Department of Chemistry and Cherry Emerson Center for Scientific Computation, Emory University, Atlanta, GA, 30322

(Dated: January 13, 2025)

Topological matter shows promise for applications in quantum information and transport. In this work, we examined the electronic and vibronic properties of a prototype molecular system adsorbed to the edges, domain walls, and the bulk of a Su-Schrieffer Heger polyacetylene chain in the trivial, metallic, and topological phases. Our results reveal that suitable molecular observables show signatures of the topological phase transition and imply the topological phase has a significant advantage and robustness over the metallic phase for electron donation into the molecular system. This advantage persists in the presence of defects and suggests applications of topological materials in molecular catalysis and sensing.

I. INTRODUCTION

Topological insulators are phases of matter with a bulk band gap and gapless surface states protected by global symmetries [1–7]. These materials show intriguing properties, such as high surface carrier mobility [8–14] with low power dissipation [15, 16], and spin-polarized current with unconventional texture [17–20]. Potential applications have been explored for spintronics [21–25], quantum computing [22, 26, 27] and thermoelectrics [28–32]. Recently, there has also been interest in the utilization of topological insulators and semimetals in electrochemistry and chemical catalysis [33–37]. The highly localized conducting boundary modes may significantly influence surface reactions, and their properties are topologically protected (robust) from local perturbations (e.g., lattice defects and impurities). For instance, high surface carrier mobility materials are desired for photocatalytic reactions as highly efficient electron-hole pair generation and recombination suppression contribute to enhanced efficiency [33, 38–40]. Recent experimental [41–45] and computational [46, 47] work has provided evidence that topological matter gives enhanced reactivity mediated by topologically protected boundary electrons. Despite these findings, the extent to which the surfaces of topological materials can be employed to achieve high-efficiency selective synthesis remains open.

In heterogeneous catalysis, adsorbed molecules undergo several processes on a solid surface [48–52]. An important step is charge transfer between the extended material and the adparticles [53–55]. Orbital hybridization and electron donation into a molecular system influences its adsorption [48, 56, 57], surface diffusion [58, 59], and desorption while potentially reducing energetic barriers for bond-breaking or association [60, 61]. Similarly, adsorbate-surface energy exchange via molecular vibrational energy relaxation and excitation of boundary electron-hole pairs (EHPs) [62–70] have been suggested to play a fundamental role in H_2 relaxation on metal surfaces [71, 72], CO_2 reduction [73–76] and water oxidation

[77].

In this work, we employed the Su-Schrieffer-Heeger (SSH) model [78, 79] to provide a comparative analysis of the interaction of topological, metallic, and trivial insulator phases with prototype molecules. We analyzed the electron occupancy of the lowest unoccupied molecular orbital (LUMO) for various configurations of single or multiple adsorbates and the different electronic phases of the SSH chain in the presence and absence of trivial and topological defects. Manifestations of the topological phase transition on the electronic friction of an adsorbate [62, 66] are also reported. The results reveal a robust advantage of the topological phase over the metallic for charge hybridization and significant enhancement of the electronic friction in the topological phase relative to the trivial insulator.

We analyzed the electron occupancy of the lowest unoccupied molecular orbital (LUMO) for various configurations of an adsorbate and electronic phases of the SSH chain in the presence and absence of trivial and topological defects. This approach is motivated by studies on ladders, where long-lasting hybridization between a discrete level (impurity state) and a continuum with bound states has been observed [80]. Visuri et al. investigated the time-dependent occupation of such a system and introduced the concept of "return probability" as a measure of the bound state existence and localization properties. We aim to leverage similar insights into the context of topological phases with molecules and defects.

This article is organized as follows. In Sec. II, we describe the employed effective Hamiltonian of the adsorbate-chain system and formally introduce the molecular observables and configurations investigated in this work. In Sec. IIIA, we present and explain our observations of topologically enhanced chemisorption. In Sec. IIIB, we systematically analyze the mean LUMO electron occupancy in the presence of a variable concentration of molecules and defects. Sec. IIIC discusses electronic friction in the topological, trivial, and metallic phases. We summarize our main results and comment on future directions in Sec. IV. Appendix A includes a detailed discussion of the numerical method used to compute the electronic friction.

* raphael.ribeiro@emory.edu

II. THEORY

A. Fano-Anderson SSH model

Our simplest considered system consists of a molecule adsorbed to different regions of an open conjugated chain (Fig. 1). The isolated molecule has a closed shell and a single low-lying electronic orbital, while the SSH chain models the extended material [78, 81]. The molecular subsystem interacts with the closest atoms of the solid-state material as in the Fano-Anderson model [63, 82]. To examine the role of bulk and boundary modes on molecular observables, we place the molecule at the center or near the edges of the material (Fig. 1).

The SSH model represents a polyacetylene chain by a 1D tight-binding lattice with two identical sites per unit cell, nearest-neighbor staggered hopping [78], and one electron per site. For a spinless open system, the isolated chain electronic Hamiltonian is given by

$$\hat{H}_{\text{SSH}} = v \sum_{j=1}^N \left(\hat{d}_{j,B}^\dagger \hat{d}_{j,A} + \hat{d}_{j,A}^\dagger \hat{d}_{j,B} \right) + w \sum_{j=1}^{N-1} \left(\hat{d}_{j+1,A}^\dagger \hat{d}_{j,B} + \hat{d}_{j,B}^\dagger \hat{d}_{j+1,A} \right), \quad (1)$$

where v (w) is the intracell (intercell) electron hopping, N is the number of unit cells, and $\hat{d}_{j,\alpha}^\dagger$ ($\hat{d}_{j,\alpha}$) is the fermionic creation (annihilation) operator in the sublattice $\alpha \in \{A, B\}$ at the unit cell j . The gapped phases of the SSH model correspond to $v \neq w$, with $v > w$ corresponding to a trivial insulator with no boundary-localized modes. In contrast, $v < w$ gives a gapped system with two zero-energy boundary-localized modes [4] (at the middle of the gap between the valence and conduction bands).

The electronic Hamiltonian of an isolated effective single-level adsorbate (adparticle) is given by $\hat{H}_0(R) = \epsilon_0(R) \hat{d}_0^\dagger \hat{d}_0$, where d_0 is the electronic annihilation operator for the adsorbate orbital (LUMO) with energy $\epsilon_0(R)$ parametrized by an internal molecular coordinate (e.g., a normal-mode displacement from the electronic ground-state equilibrium geometry) R . The total Hamiltonian for a single species adsorbed to the SSH chain is

$$\hat{H}(R, x_M) = \hat{H}_{\text{SSH}} + \hat{H}_0(R) + \hat{W}(x_M), \quad (2)$$

where $x_M \in \{x_B, x_E\}$ is a binary adsorbate position relative to the SSH chain, such that $x_M = x_B$ represents the system configuration where the adparticle interacts only with bulk sites (Fig. 1), whereas $x_M = x_E$ represents interaction with the (left) edge (Fig. 1). The electronic interaction Hamiltonian $\hat{W}(x_M)$ describes electron hopping between the chain and the adsorbate orbital and is

given by

$$\hat{W}(x_E) = T_{1,A} \hat{d}_{1,A}^\dagger \hat{d}_0 + T_{1,B} \hat{d}_{1,B}^\dagger \hat{d}_0 + \text{h.c.}, \quad (3)$$

$$\hat{W}(x_B) = T_{N/2,A} \hat{d}_{N/2,A}^\dagger \hat{d}_0 + T_{N/2,B} \hat{d}_{N/2,B}^\dagger \hat{d}_0 + T_{N/2-1,B} \hat{d}_{N/2-1,B}^\dagger \hat{d}_0 + \text{h.c.}, \quad (4)$$

where h.c. means Hermitian conjugate, we assumed for simplicity that the total number of unit cells N is even, and $T_{N/2,\alpha}$ is a real positive constant coupling the LUMO and the sublattice α at unit cell $N/2$ (SSH chain center). Except where otherwise mentioned, the adsorbate-chain couplings $T_{s,\alpha}$ ($s = 1, N/2$ or $N/2 - 1$ and $\alpha = A$ or B) are assumed much smaller than the intracell and intercell hopping v and w , respectively. Fig. 1 summarizes the examined configurations.

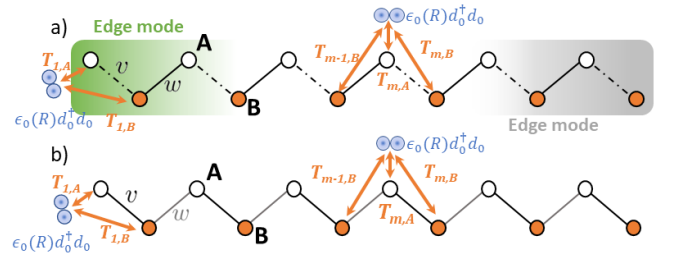


FIG. 1. Schematic representation of the studied Fano-Anderson SSH model. White and orange circles are sites on sublattices A and B, each hosting a single p_z orbital. Intra and intercell hopping amplitudes (v and w , respectively) are assumed to be tunable. The adsorbate is represented by a diatomic molecule near the edges ($x_M = x_E$) or at the bulk of the SSH chain ($x_M = x_B$). a) Adsorbate hybridization with edge or bulk modes of the topological phase ($v < w$). b) Adsorbate hybridization with a trivial insulator ($v < w$) or metallic ($v = w$) phase, where all states of the chain are maximally delocalized (metallic phase).

Polyacetylene chains typically host trivial and topological lattice defects [78, 79]. The latter defects correspond to domain walls separating the trivial ($v > w$) and topological ($v < w$) insulator phases and support robust localized (mid-gap) modes. Therefore, we also examined the scenario where multiple molecules interact with lattice defects of the SSH chain. In the static limit (where lattice defects are immobile), N_d solitons centered at m_1, m_2, \dots, m_{N_d} can be represented by a modification of the SSH Hamiltonian (Eq. 1) where the nearest-neighbor hopping amplitudes are site-dependent and given by [78]

$$t_n \equiv \tilde{H}_{\text{SSH}}^{n,n+1} = \frac{w+v}{2} + \frac{v-w}{2} \sum_{i=1}^{N_d} \phi_n^{(m_i)}, \quad (5)$$

where $\tilde{H}_{\text{SSH}}^{n,n+1}$ is the $(n, n+1)$ matrix element of the SSH Hamiltonian including N_d solitons, and $\phi_n^{(m_i)}$ is given by

[83]

$$\phi_n^{(m_i)} = (-1)^n \tanh\left(\frac{n - m_i}{\xi}\right), \quad (6)$$

where ξ is the soliton width. In our simulations of disordered samples, the adparticles form a subensemble with a noninteracting Hamiltonian \hat{H}_0 that is a simple generalization of $\hat{H}_0(R)$. Each adparticle is placed at the center of a soliton and interacts with the nearest site with coupling strength T_{m_i} as well as the nearest-neighbors $m_i - 1$ and $m_i + 1$ with lower coupling constant $T_{m_i}/3$, so each adparticle interacts with a total of three sites.

B. Observables

To characterize the hybridization and charge-transfer occurring between the different electronic phases of the SSH model and a single adsorbate, we computed the electronic population [84–86] $n_0(R, x_M)$ of the adsorbate LUMO under interaction with the half-filled SSH chain with zero Fermi energy,

$$n_0(R, x_M) = \sum_{\lambda=1}^N |\langle \lambda | \varepsilon_0 \rangle|^2, \quad (7)$$

where $\{|\lambda\rangle\}$ is the set of single-particle eigenstates of \hat{H} with energies $\{\epsilon_\lambda\}$, and $|\varepsilon_0\rangle = \hat{d}_0^\dagger |0\rangle$ where $|0\rangle$ is the global ground-state. The LUMO occupation number quantifies the charge donated by the chain to the molecular system. We employ numerical diagonalization and perturbation theory below to obtain $n_0(R, x_M)$ under various conditions of the SSH chain.

Our simulations of multiple adsorbates in the presence of a variable number of topological defects allowed us to also assess the chemisorption of a variable number of randomly placed adparticles at the center of $N_d > 1$ solitons. For these systems, we compute the LUMO occupation number

$$\bar{n}_0 = \frac{1}{N_{\text{ad}}} \sum_{i=1}^{N_{\text{ad}}} n_{0i}, \quad (8)$$

where n_{0i} is the occupation number of the i th adsorbate LUMO.

The analysis of the electronic occupation number of the adsorbate system focuses on charge transfer between the various phases of the SSH chain and a static internal configuration of the adsorbates (R fixed) positioned near the edge and bulk regions of the solid. We also explored a dynamical observable to examine the impact of the electronic interaction between the conjugated chain and the molecular system on intramolecular vibrational dynamics. We introduced a vibrational degree of freedom coupled to the adsorbate LUMO, which enables the molecular system to exchange vibrational energy with electron-hole pairs of the SSH chain.

The internal molecular vibrational degree of freedom corresponds to a harmonic oscillator with effective mass m , angular frequency ω , and displacement from equilibrium R . The electronic ground-state (unoccupied LUMO) equilibrium configuration corresponds to $R = R_0 = 0$. In contrast, when the LUMO is occupied, the minimum is displaced and located at $R_1 = -g\sqrt{\frac{2\hbar}{m\omega}}$ (g parametrizes the relative separation of equilibrium geometries with empty and filled LUMO). In this scenario, the isolated adsorbate electronic-vibrational Hamiltonian is given by [52, 63, 64, 87, 88]

$$\begin{aligned} \hat{H}_0(R) &= \varepsilon_0(R) \hat{d}_0^\dagger \hat{d}_0 + U_0(R), \\ &= \left(\varepsilon_d + gR\sqrt{\frac{2\hbar}{m\omega}} \right) \hat{d}_0^\dagger \hat{d}_0 + \frac{m\omega}{2\hbar} R^2, \end{aligned} \quad (9)$$

where ε_d is the LUMO energy at $R = 0$, and $U_0(R)$ is the isolated adparticle electronic ground-state (zero LUMO occupation number) potential energy curve for vibrational motion.

In the presence of interactions with an extended electronic material, vibrational relaxation of the molecular system can happen via non-adiabatic electron-hole pair excitation [62, 89]. Under the assumption that the electronic subsystem relaxes to its thermal equilibrium state much faster than adsorbate-boundary dynamics [90, 91], the energy exchange between vibrational degrees of freedom of the adsorbate and the electron-hole pairs of the solid-state system can be quantified by the electronic friction tensor [62, 66, 92–94]. For an adsorbate with a single vibrational degree of freedom, the friction coefficient $\gamma(R)$ can be written as [66, 88, 95]

$$\gamma(R) = -\pi\hbar \int_{-\infty}^{\infty} d\epsilon \Xi(\epsilon; R) \frac{\partial f_T(\epsilon)}{\partial \epsilon} \quad (10)$$

$$\Xi(\epsilon; R) = \text{Tr}_m \left[\frac{\partial \hat{H}(R)}{\partial R} \hat{P}(\epsilon; R) \frac{\partial \hat{H}(R)}{\partial R} \hat{P}(\epsilon; R) \right] \quad (11)$$

where Tr_m implies trace over the electronic orbitals, $f_T(\epsilon)$ is the Fermi-Dirac distribution at temperature T , and $P(\epsilon, R) = \sum_\lambda \delta[\epsilon - \epsilon_\lambda(R)] |\lambda; R\rangle \langle \lambda; R|$, where $|\lambda(R)\rangle$ correspond to electronic adiabatic levels at the adsorbate geometry R . For the Hamiltonian in Eq. (2) with $\hat{H}_0(R)$ given by (9), we can write the electronic friction coefficient in a simpler form

$$\begin{aligned} \gamma(R) &= -\pi\hbar \left[\frac{\partial \varepsilon_0(R)}{\partial R} \right]^2 \int_{-\infty}^{\infty} d\epsilon \sum_{\lambda\lambda'} |\langle \lambda; R | \varepsilon_0(R) \rangle|^2 \\ &\quad \times \delta[\epsilon - \epsilon_\lambda(R)] |\langle \lambda'; R | \varepsilon_0(R) \rangle|^2 \delta[\epsilon - \epsilon_{\lambda'}(R)] \frac{\partial f_T(\epsilon)}{\partial \epsilon}. \end{aligned} \quad (12)$$

Since our interest lies in thermodynamic limit behavior, we approximate the discrete electronic state manifold $\{|\lambda(R)\rangle\}$ by a continuous set of electronic states via

replacement of $\delta(\epsilon - \epsilon_\lambda)$ by a Gaussian distribution centered at ϵ_λ with width σ [95, 96]

$$\delta(\epsilon - \epsilon_\lambda) = \frac{1}{\sigma\sqrt{2\pi}} \exp\left[-\frac{(\epsilon - \epsilon_\lambda)^2}{2\sigma^2}\right]. \quad (13)$$

We choose σ to correspond to half the energy difference between the HOMO and LUMO of the (isolated) half-filled SSH chain in the metallic phase. This choice leads to the smooth friction coefficients computed in Sec. III C.

III. RESULTS AND DISCUSSION

A. Bulk and boundary chemisorption

In this section, we examine the chemisorption of the adparticle on the SSH chain under various conditions. Figures 2(a) and (b) report the occupation number $n_0(R, x_M)$ of the adparticle LUMO when it is near the boundary ($x_M = x_E$) or the bulk ($x_M = x_B$) of the conjugated chain in the trivial, topological and metallic electronic phases for various LUMO energies ϵ_0 . Throughout this section, we ignore the dependence on R_0 , i.e., the adparticle is characterized by its LUMO energy ϵ_0 and its position relative to the chain.

Figure 2(a) shows that while the trivial insulator phase has no capability for electron sharing, the topological phase strongly interacts with the LUMO, leading to a sharp change in $n_0(R, x_E)$ at the onset of the topological phase transition. This occurs especially when the LUMO is nearly resonant with a boundary mode. Conversely, Fig. 2(b) shows when the adparticle is near the SSH bulk, the LUMO occupation is only significant when the chain is in a small neighborhood of the critical (phase transition) point, where the density of occupied electronic states with energy close to ϵ_0 is maximized. Notably, while Fig. 2 evidences the metallic phase is the most favorable for bulk adsorption, boundary chemisorption in the topological phase is still the optimal considered scenario for chemisorption as $\max n_0(R, x_B) < \max n_0(R, x_E) = 0.5$. Furthermore, significant electron sharing between the boundary mode of the conjugated chain and the LUMO persists even when $\epsilon_0 \gg 0$.

We highlight the robustness of the topological enhancement in Fig. 3, where we directly compare the ability of the metallic and topological phases to share electrons with the LUMO at variable ϵ_0 and LUMO-chain hopping amplitudes. In all examined cases, hybridizing the adparticle with the bulk metallic states leads to lower LUMO electron occupancy than the topological phase, despite the substantially higher density of metallic states nearly resonant with the LUMO. The topological phase leads to significant $n_0(R, x_E) \neq 0$ even when $T_{1,A} \ll v, w$, thus demonstrating the effectiveness of LUMO hybridization with the SSH edge modes under a variety of conditions.

The behavior of $n_0(R, x_E)$ in the topological phase can be understood with perturbation theory. In the near-resonant case ($\epsilon_0(R) \approx 0$), the Hamiltonian for the isolated molecule and chain is (quasi)-threefold-degenerate, but only the (initially occupied by assumption) left boundary mode interacts with the adparticle. This leads to significant hybridization between the LUMO and the nearest edge mode, which is only weakly perturbed by the bulk valence and conduction states when $|w/v - 1| \gg 0$. For $T_{1,A}, T_{1,B} \ll w, v$ and $\epsilon_0 \approx 0$, the adsorbate-edge hybrid remains isolated with energy approximately equal to $-T_{1,A}\alpha_1$, where α_1 is the amplitude of the edge mode at the sublattice A of the first unit cell. This leads to $n_0(R, x_E) \approx 0.5$ as shown in Fig. 2.

In the metallic phase ($v \approx w$), the LUMO is near degenerate with many occupied and unoccupied states when $\epsilon_0(R) \approx 0$. As such, while Fig. 2(b) shows $n_0(R, x_B)$ is maximized at the critical point of the topological phase transition ($v \approx w$), the LUMO occupation number is approximately 0.4. This feature arises from the asymmetric line shape in the local molecular density of states originating from the LUMO hybridization with

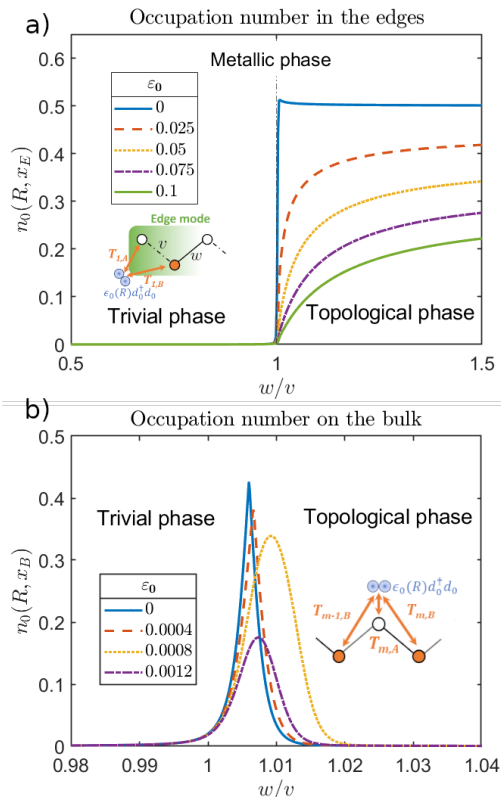


FIG. 2. Occupation number of a low-lying adsorbate orbital near the (a) edge ($T_{1,A} = T_{1,B}/3 = 0.1$) and (b) bulk ($T_{N/2,A} = T_{N/2+1,B}/3 = T_{N/2-1,B}/3 = 0.1$) of the conjugated chain in the trivial ($v > w$), metallic ($w/v \approx 1$) and topological ($w > v$) phases for a system with $N = 800$, $v = 10$ and $E_F = 0$.

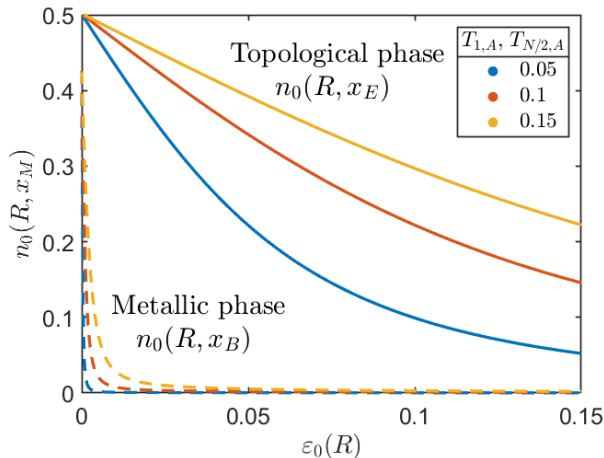


FIG. 3. LUMO occupation number vs adsorbate orbital energies ε_0 for adsorption to the left boundary of the topological phase with $w = 15$ (solid lines), and bulk of metallic phases [as identified by the peak in $n_0(R, x_B)$, see Fig. 2(b)] with $w = 10.0814$ (blue), 10.0597 (red) and 10.0465 (yellow) for various molecule-adsorbate hopping amplitudes $T_{m,A}$. The remaining parameters are $N = 800$, $v = 10$, and $E_F = 0$.

the metallic quasi-continuum around $E_F = 0$ [82].

In the off-resonant case where $\varepsilon_0 \gg E_F$, the electronic occupancy of the adsorbate LUMO near the bulk of the sample can be approximated using perturbation theory

$$n_0(R, x_B) = \sum_{\kappa} \left| \frac{T_{N/2,A} a_{N/2,\kappa} + T_{N/2,B} b_{N/2,\kappa} + T_{N/2-1,B} b_{N/2-1,\kappa}}{\varepsilon_0 - E_{\kappa}^{(0)}} \right|^2, \quad (14)$$

where $a_{N/2,\kappa}$ ($b_{N/2,\kappa}$) is the probability amplitude for the SSH κ state on unit cell $N/2$ in sublattice A (B), and $E_{\kappa}^{(0)}$ is the corresponding unperturbed energy of the bare κ level. The sum is over the N lowest single-particle states of the SSH chain. It follows from Eq. (14) that when $\varepsilon_0 > 0$ and the chain is in the trivial or topological phases, $n_0(R, x_B)$ approximately vanishes everywhere except for a small region around $w/v \approx 1$. This occurs because when $w/v < 1$ or $w/v > 1$, the occupied chain states with significant electron amplitude near the molecule are delocalized across the entire chain, and especially for small and large w/v , there is a significant gap between these extended modes and the LUMO when ε_0 is close to $E_F = 0$ as investigated here. Conversely, the metallic phase favors a greater LUMO occupation number when the adsorption occurs at the bulk of the chain, as near the critical point of the topological phase transition, a greater density of states exists near the LUMO energy. This feature leads to smaller denominators in Eq. (14) and greater $n_0(R, x_B)$.

In summary, we find that the strong localization of

midgap modes of the topological phase enables more significant and robust hybridization and charge donation by the half-filled SSH chain into an adsorbate localized near an occupied boundary mode of the chain. Despite its greater density of electronically occupied levels, the metallic phase shows weaker hybridization and charge transfer into the LUMO due to the local nature of the adsorbate-chain interactions.

B. Chemisorption on solitons and trivial defects

The topological phase only hosts zero-energy modes at the boundaries of the pristine SSH chain, but bulk topological defects (solitons) are generic at finite temperature and host additional localized states in the bulk of the chain, which can also efficiently share electrons with a nearby adsorbate. Similarly, given the advantage of the topological phase over metallic for chemisorption arises from the interaction of strongly localized mid-gap modes of the former with a nearby adsorbate, it is conceivable that the introduction of trivial defects (represented by dopants occupying sites of the SSH chain with random on-site energy around 0) in the metallic phase will lead to a disordered metallic phase with enhanced charge donation into adparticles just as the topological phase. In this subsection, we analyze electronic hybridization and charge donation between multiple adsorbates and SSH chains hosting topological defects. We contrast these scenarios with those where multiple adsorbates are placed near trivial defects of the SSH chain in the metallic phase.

We computed the average LUMO electron occupancy, \bar{n}_0 (Eq. 8), for a system including N_{ad} adparticles interacting with a soliton ensemble randomly distributed along the SSH chain. Each molecule is adsorbed to the center of a topological defect, and we assume the total number of adparticles is the same as the number of topological defects (including left and right boundaries). We also explored the dependence of \bar{n}_0 on the soliton width $\xi = \{5, 7, 10\}$ as the localization length of the midgap mode produced by each domain wall strongly depends on its width. For comparison, we also examined the mean LUMO occupation number obtained for the case where the adsorbates are near trivial defects of a disordered

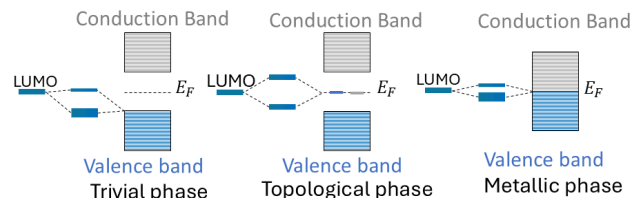


FIG. 4. Electronic hybridization of the adsorbate LUMO state and the polyacetylene on the trivial (left), topological (center) and metallic (right) phase.

metallic chain. Finally, we also compare the case where the adsorbates are randomly placed near bulk sites of the pristine SSH chain in the metallic phase ($w/v = 1$). In all simulations, the the electronic ground-state configuration is obtained assuming a fixed number of N electrons originating from the SSH chain with N unit cells (half-filling).

We observe consistently greater \bar{n}_0 in the SSH chain filled with topological defects relative to the metallic phase with trivial defects. Figure 5a shows the average LUMO occupation number as a function of adsorbate number, \bar{n}_0 for the case where the LUMO energy is $\varepsilon_0 = 0$ for variable ratios of inter to intracell hopping (w/v) and

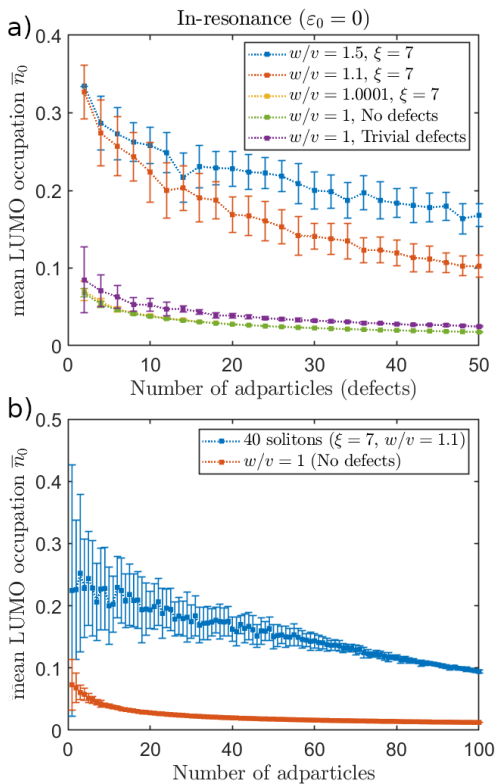


FIG. 5. Mean occupation number of adparticle LUMO when in-resonance with mid-gap zero-modes of the SSH chain with variable defect number. In a), we show \bar{n}_0 obtained for a system of adsorbates, each placed near the center of a soliton ($w/v = 1.5, 1.1$ and 1.0001), trivial defect (in the metallic case $w/v = 1$ with trivial defects), or randomly in the bulk of the chain ($w/v = 1$ case with no defects). In b), the adparticles are placed near random sites of the chain, and we present, for a fixed number of 40 solitons in the topological phase and the clean metal phase, the mean occupation number of the adsorbate LUMO as a function of the number of adsorbates. In all computations, the soliton width was set to $\xi = 7$, $N = 3000$, $v = 10$, $T_m = 0.1$, and each point corresponds to an average of 25 realizations.

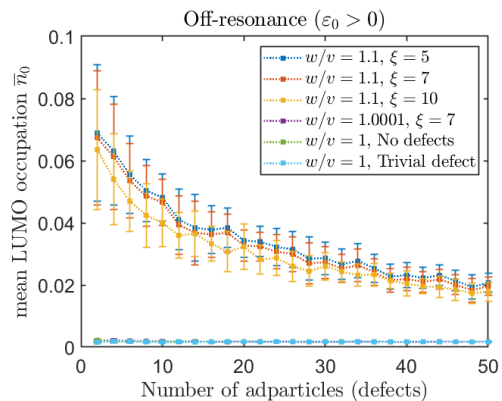


FIG. 6. Off-resonance mean occupation number of adparticle LUMO $\varepsilon_0 > 0$ under interaction with SSH chains containing a variable number of defects as a function of the number of adparticles. The total number of unit cells is $N = 3000$, $\varepsilon_0 = 0.1$, $v = 10$, $T_m = 0.1$.

therefore soliton width (Eq. 6). The vertical lines represent the standard deviation of the electron occupancy for each number of solitons (or adsorbates since the number of adparticles is equal to the number of solitons in each case examined in this figure). The topological phase with domain walls showed enhanced electron transfer due to the highly localized zero-energy solitons.

Note that at half-filling (i.e., with $2N$ electrons originating from an SSH chain with N unit cells), only half of the solitons/antisolitons donate electrons to the LUMO adparticles. At small numbers of soliton-antisoliton pairs, the electron transfer average is dominated by the contributions of the edge modes. However, the average occupation number approaches the soliton electron donation for more significant numbers of solitons, where the soliton localization is significantly smaller than the edge modes. The electron donation is enhanced for greater intercell hopping w , indicating a higher soliton localization, consistent with early literature [78]. In the near-critical case of $w/v = 1.0001$, charge transfer by the topological zero-energy mid-gap states near-resonant with adsorbates is reduced to greater delocalization of topological defect states.

We also computed the mean electron occupancy of a random distribution of adparticles with a fixed number of solitons (50 solitons/antisolitons) at various concentrations of adparticles. Figure 5 b) shows a direct comparison of the metallic phase (no defects) and a polyacetylene chain with equally spaced domain walls with near-zero overlap. The molecules were randomly distributed along the SSH chain with a LUMO energy $\varepsilon_0 = 0.001$. At small concentrations of adparticles, the mean electron occupancy hovered around 0.25. This behavior arises because adparticles primarily exist in one of two states: interacting with a soliton, leading to an occupancy of 0.5, or not interacting, resulting in an occupancy close to zero. Furthermore, we observed a significant decrease in the mean electron occupancy for the metallic phase compared to

the topological phase with domain walls, highlighting a distinct advantage of the topological defects. Moreover, the difference in mean electron occupancy between the metallic phase and domain walls remained prominent at high electron concentrations, further topological signatures of domain walls via electron donation. This phenomenon elucidates the significant impact of adparticle saturation on the reduction of the mean electron occupancy, emphasizing its crucial role in modulating electronic properties.

Fig. 6 also reports the relationship between the mean LUMO occupation \bar{n}_0 and the soliton width ξ . As illustrated in Figure 6, the mean electron occupancy slightly depends on the soliton width, wherein a narrower domain wall width ξ results in an augmented mean electron donation into the LUMO adparticles. This is attributed to the heightened localization of solitons at reduced widths, leading to an increased overlap with the adparticles and, consequently, a more pronounced adsorbate-chain orbital hybridization. Moreover, the average electron donation in the trivial defects/nearly metallic phase is similar to the metallic phase, signifying the influence of domain walls in the off-resonance case on electron transfer.

C. Topological phase transition signature on electronic friction

Using the adiabatic electronic orbitals obtained from diagonalization of the Hamiltonian given by Eq. (2) with $\varepsilon_0(R) = \varepsilon_d + Rg\sqrt{m\omega/\hbar}$, we find the local density of states $P(\varepsilon, R)$ and compute the electronic friction, Eq. (12), at the trivial, topological insulator, and metallic phases of the SSH chain at finite temperature $1/\beta = 0.015$. As discussed in Sec. II, $P(\varepsilon, R)$ is smoothed using Gaussian lineshapes centered at each adiabatic orbital energy $\varepsilon_\lambda(R)$ with bandwidth $\sigma = 0.019$. This choice is not unique [95], but it provides smooth (non-oscillatory) $P(\varepsilon, R)$ and $\gamma(R)$, allowing us to derive qualitative relations between the behavior of $\gamma(R)$ in the three electronic phases. See Appendix A for electronic friction calculations at different bandwidths. For a small density of impurities in the system and a fixed number N of electrons in the polyacetylene chain, we can approximate the system as an intrinsic semiconductor [97]. We treat the interacting adparticle as a hole impurity setting the Fermi level E_F at the HOMO-LUMO mid-gap energy at half-filling (with N valence spinless electrons). Therefore, E_F varies with the molecular coordinate R (see Fig. 8 b).

In Fig. 7a, we present the electronic friction as a function of the adparticle LUMO energy, $\varepsilon_0(R)$, when the molecule is positioned near the edges and the bulk of the SSH chain in the topological ($w/v = 1.1$), metallic ($w/v = 1$), and trivial ($w/v = 0.9$) phases. The extended material consists of $N = 800$ unit cells, $v = 10$,

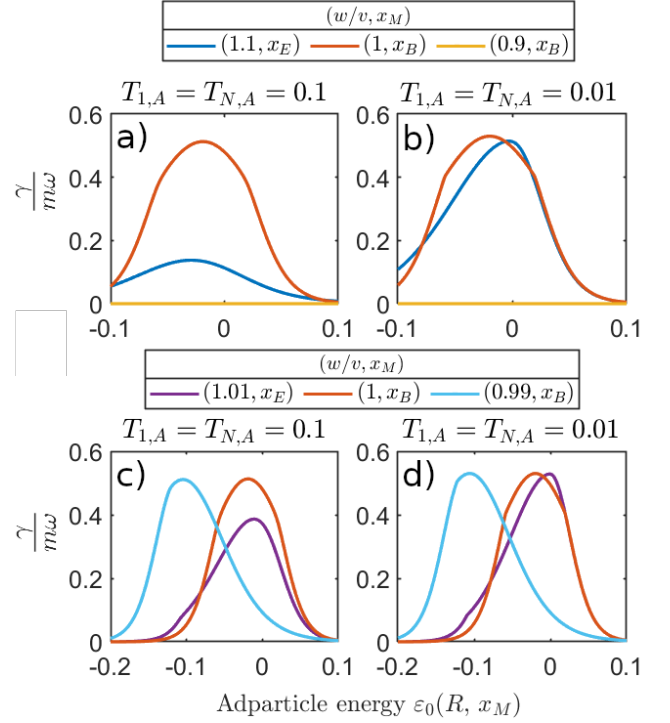


FIG. 7. Electronic friction (12) of polyacetylene chain under interaction with an adparticle for the Hamiltonian (2). Electronic friction in the topological phase $w/v = 1.1$ in the edges (x_E), and metallic $w/v = 1$ and trivial insulator $w/v = 0.9$ in the bulk (x_B) at a) $T_{1,A} = T_{N/2,A} = 0.1$, and b) $T_{1,A} = T_{N/2,A} = 0.01$. Figures c) and d) refer to the electronic friction near the phase transition at $T_{1,A} = T_{N/2,A} = 0.1$, and $T_{1,A} = T_{N/2,A} = 0.01$, respectively. The parameters are chosen were $v = 10$, $\sigma = 0.019$, $\varepsilon_d = 0.15$, $g = 0.02$, $\beta = 1/0.015$, $N = 800$ (number of unit cells), and $T_{N/2-1,B} = T_{N/2,B} = T_{N/2,A}/3$.

and $g = 0.02$ at temperature $1/\beta = 0.015$. We observe higher electronic friction in the metallic phase due to numerous strongly interacting bulk states near the Fermi level. The friction curve in the metallic phase is shifted to lower energies due to the creation of electron-hole pairs in the valence band, thus lowering the Fermi energy. In the vicinity of the edges within the topological phase (depicted as a solid blue line), the interaction between the localized edge mode and the molecule increases the electronic friction, although to a lesser extent than in the metallic phase. The reduced value of $\gamma(R)$ in the topological phase, relative to the metallic phase, arises from the energy splitting $2O(T_{1,A})$ between the interacting edge mode and the in-resonance LUMO adparticle level. This is shown in Fig. 8a which shows in the molecular projected DOS $\langle \varepsilon_0 | P(\varepsilon, R) | \varepsilon_0 \rangle$ the splitting of the edge mode and the LUMO adparticle arises from the low electronic density of the interacting boundary modes of the 1D SSH chain. Notably, in 2D and 3D topological systems, the energy splitting of the edge modes and the adparticle is expected to be reduced by the greater elec-

tronic density of boundary modes, enhancing the electronic friction.

Figure 7b illustrates higher electronic friction $\gamma(R)$ at smaller coupling, $T_{1,A} = 0.01$, due to the reduction in energy splitting between the edge mode and the LUMO molecular level. Refer to Appendix A to see the energy splitting of the PDOS at different coupling parameters $T_{1,A}$. This splitting results in a low local density of states at the Fermi energy, suppressing the electronic friction by limiting the availability of low-lying electronic transitions for electron-hole pair formation near the Fermi level.

For a sufficiently large polyacetylene band gap ($w-v = 1$), the thermal fluctuations of the SSH electronic manifold (valence band) in the trivial phase are energetically far from the LUMO energy, as depicted in Fig. 8b. This separation is due to the Fermi energy being set to the HOMO-LUMO mid-gap of the hybridized particle-SSH chain complex, as previously discussed. Consequently, there is no electronic friction for the LUMO adparticle in the trivial phase. Note that the electronic friction in the topological phase interacting in the bulk resembles the results of the trivial phase, that is, the calculations were omitted in Fig.7. Importantly, Fig. 7a and b show the electronic friction vanishes in the trivial phase (yellow line), thus demonstrating another signature of topological phase transition via the vibrational relaxation of an adsorbed particle. For such cases, the dominant energy dissipation in gapped systems is via phonon-induced excitations in the insulator substrate [98, 99].

Figure 7c compares the electronic friction near the phase transition as a function of the adparticle LUMO energy, $\varepsilon_0(R)$, at $T_1 = 0.1$. In the topological phase, the electronic friction increases due to the electronic contributions of the conduction and valence bands to the local density of states, $P(\varepsilon, R)$, of the LUMO adparticle. Conversely, in the trivial phase, the peak of the electronic friction shifts towards the valence bands due to the dependence of the Fermi level on the HOMO-LUMO gap. Thus, the electronic friction peak is centered when the adparticle energy matches the polyacetylene HOMO energy, approximately $\varepsilon_0(R) \approx w - v \approx -0.1$ at $v/w = 9.9$. This observation highlights the signatures of phase transition through the adsorbate dynamics and the influence of topological boundary modes on the vibrational relaxation process. Similar to Fig. 7b, the energy splitting is suppressed for small coupling, T_1 , even when the electronic conduction and valence band states are coupled with the hybrid adparticle-edge mode states.

IV. CONCLUSIONS

Our analysis of the interaction of prototype molecules with an empty level with the SSH polyacetylene chain shows a robust advantage for the electron donation into a LUMO adsorbate in the topological phase over the metallic and trivial insulator phases - this advantage of the

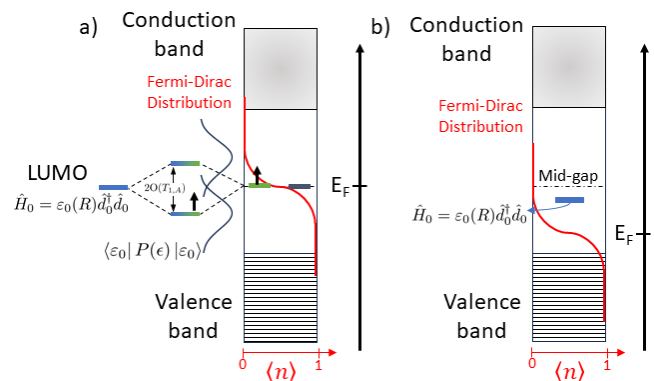


FIG. 8. a) Electronic level coupling of the adsorbed particle and the SSH chain in the topological phase. The hybrid edge mode and LUMO adparticle produce a projected DOS $\langle \varepsilon_0 | P(\varepsilon, R) | \varepsilon_0 \rangle$ with two peaks split by $2O(T_{1,A})$. The interaction with the right edge mode is zero. b) Trivial insulator phase coupling of the adsorbed particle and the SSH chain. At half-filling, the Fermi energy E_F is set as the mid-gap of the HOMO-LUMO gap.

topological phase results from the strong localization of charge carriers near the edges that is afforded by the topological phase. Intriguingly, while the metallic phase shows a greater density of states near the Fermi energy, the large delocalization of the bulk modes suppresses the local charge transfer interaction and leads to weaker hybridization between the metallic phase and the localized atomic system. We also showed that the localized mid-gap modes created by topological bulk defects (domain walls) lead to substantially greater efficiency in charge donation relative to the metallic phase with trivial imperfections. This indicates that the presence of localized modes is necessary but not sufficient condition for enhanced electronic hybridization between the SSH chain and localized atomic systems. The topological character of the mid-gap states plays an essential role.

Our analysis of the electronic friction generated by the non-adiabatic interaction of the SSH chain with an adsorbate revealed that the topological phase transition is clearly manifested in this quantity. Indeed, these results suggest that the study of the molecular vibrational relaxation process (electronic friction) manifests the presence of topologically protected mid-gap states. In particular, the electronic friction is significantly more potent in the topological insulator relative to the trivial insulator phase. However, the metallic phase shows the greatest friction since it contains the largest density of electronic states near the Fermi energy, and the electronic friction is greatly sensitive to this quantity. These findings suggest that topological insulators, particularly those with highly localized surface states and a higher density of states near the Fermi energy, such as Weyl semimetals, could offer significant advantages for molecular vibrational relaxation. This could lead to new applications of topological materials for catalysis and surface chemistry.

Appendix A: Electronic friction bandwidth

In our study, we expand the delta functions in the local density of states by introducing a Gaussian bandwidth denoted as σ in Equation (13). This selection is influenced by the Wide-Band Limit (WBL) approximation, which presumes a constant density of states (DOS) near the Fermi level within the thermodynamic limits. The WBL approximation is frequently applied in the metallic phase to characterize the behavior of the electronic system, resulting in continuous DOS rather than discrete delta functions. The value $\sigma = 0.019$ that we have opted for is determined by considering the energy difference of the bare SSH chain near the Fermi energy in the metallic phase for $N = 800$ unit cells. This choice of bandwidth allows us to capture pertinent features of the DOS, encompassing the projected electronic density on the LUMO adparticle state $\langle \varepsilon_0 | P(\varepsilon, R) | \varepsilon_0 \rangle$. By utilizing a Gaussian bandwidth to broaden the delta functions appropriately, we ensure that the resultant PDOS becomes a smooth function. This facilitates comparison with the derivative of the Fermi-Dirac distribution to ascertain electronic friction, as depicted in Figure 10. Consequently, bandwidth broadening significantly affects electronic friction, as demonstrated in Figure 9, where a wider bandwidth σ suppresses electronic friction. However, our analysis and conclusions remain agnostic to bandwidth variations, as the signatures of phase transitions and topological advantages persist across different bandwidths σ .

The impact of Gaussian bandwidth broadening, σ , on electronic friction is illustrated in Figure 9. In the metallic phase, it becomes evident that reducing the bandwidth enhances the friction peak. However, under the thermodynamic limit, the WBL can be applied [100], leading to a progressively broadened DOS. In contrast, the electronic friction in the topological phase exhibits minimal sensitivity to various bandwidths. This behavior arises due to the relatively large HOMO-LUMO gap, resulting in limited overlap between the PDOS and the derivative of the Fermi-Dirac distribution.

Similarly, the interaction parameter $T_{1,A}$ in the topological phase influences the hybridization of electron-hole pairs by increasing the energy splitting between the edge

mode and the adparticle at higher $T_{1,A}$, as shown in Figure 10a. The two peaks of the continuous blue line correspond to the hybridized adparticle-edge state, exhibiting equal probability density at $\varepsilon_0 = 0$. As the Fermi energy E_F lies between these two peaks, there is a limited overlap with the derivative of the Fermi-Dirac distribution, $\frac{\partial f_F(\varepsilon)}{\partial \varepsilon}$, at $T_{1,A} = 0.1$ (continuous red line).

It is important to note that the Fermi energy in the topological phase is not defined as the mid-gap energy between the interacting edge mode and the adparticle hybrid due to the remaining non-interacting (right) edge

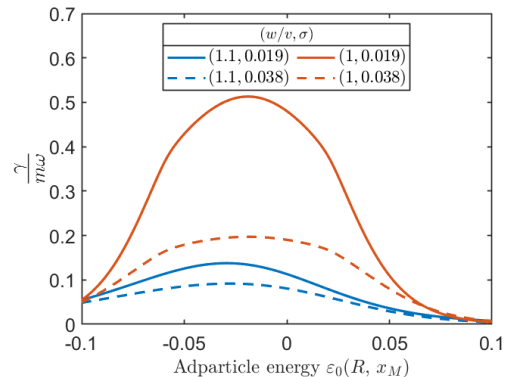


FIG. 9. Electronic friction (12) dependence on the bandwidth broadening σ at the topological phase ($w/v = 1.1$) in the edges and the metallic phase ($w/v = 1$) interacting in the bulk. We showed the dependence on the bandwidth broadening at $\sigma = 0.019$ and $\sigma = 0.038$. The parameters are $v = 10$, $T_{N/2,A} = T_{1,A} = 0.1$, $g = 0.02$, $\beta = 1/0.015$, $N = 800$ (number of unit cells), and $T_{N/2-1,B} = T_{N/2,B} = T_{N/2,A}/3$.

mode. This adjustment ensures that the Fermi energy approaches zero ($E_F = 0$) as the interaction with the chemisorbed molecule weakens ($T_{1,A} \rightarrow 0$).

For smaller coupling values ($T_{1,A}$) represented by the dashed and dotted blue lines, the two peaks overlap and center around the Fermi energy, leading to higher electronic friction. In Figure 10b, we compare the squared PDOS $|\langle \varepsilon_0 | H | \varepsilon_0 \rangle|^2$ at fixed adparticle energy $\varepsilon_0 = 0$ in the metallic phase (dashed line), where a single PDOS peak and the Fermi energy are centered at the resonance point $\varepsilon_0 = 0$.

[1] M. Z. Hasan and C. L. Kane, Colloquium: topological insulators, *Reviews of modern physics* **82**, 3045 (2010).
 [2] J. E. Moore, The birth of topological insulators, *Nature* **464**, 194 (2010).
 [3] A. P. Schnyder, S. Ryu, A. Furusaki, and A. W. Ludwig, Classification of topological insulators and superconductors in three spatial dimensions, *Physical Review B* **78**, 195125 (2008).

[4] J. K. Asbóth, L. Oroszlány, and A. Pályi, A short course on topological insulators, *Lecture notes in physics* **919**, 166 (2016).
 [5] C. L. Kane and E. J. Mele, Quantum spin hall effect in graphene, *Physical review letters* **95**, 226801 (2005).
 [6] C. L. Kane and E. J. Mele, Z₂ topological order and the quantum spin hall effect, *Physical review letters* **95**, 146802 (2005).

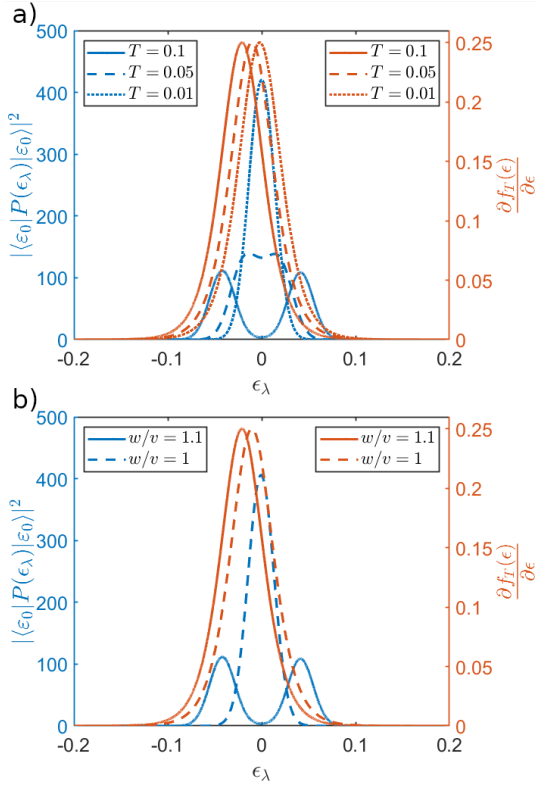


FIG. 10. Squared projected density of states on the adparticle LUMO $|\langle \epsilon_0 | P(\epsilon, R) | \epsilon_0 \rangle|^2$ at $\epsilon_0 = 0$ in the topological phase (continuous blue line) and metallic phase dotted blue line) in the edges and bulk, respectively. We included the derivative of Fermi Dirac distribution $\partial f_T(\epsilon)/\partial \epsilon$ on the right y-axis scale to show the overlap on both phases. The parameters are $v = 10$, $T_{N,A} = T_{1,A} = 0.1$, $\beta = 1/0.015$, $N = 800$ (number of unit cells), $\sigma = 0.019$, and $T_{N/2-1,B} = T_{N/2,B} = T_{N/2,A}/3$.

[7] B. A. Bernevig, T. L. Hughes, and S.-C. Zhang, Quantum spin hall effect and topological phase transition in hgte quantum wells, *science* **314**, 1757 (2006).

[8] C. Shekhar, S. Ouardi, A. K. Nayak, G. H. Fecher, W. Schnelle, and C. Felser, Ultrahigh mobility and non-saturating magnetoresistance in heusler topological insulators, *Physical Review B* **86**, 155314 (2012).

[9] C. Shekhar, S. Ouardi, G. H. Fecher, A. Kumar Nayak, C. Felser, and E. Ikenaga, Electronic structure and linear magnetoresistance of the gapless topological insulator ptusb, *Applied Physics Letters* **100**, 252109 (2012).

[10] J. G. Analytis, R. D. McDonald, S. C. Riggs, J.-H. Chu, G. Boebinger, and I. R. Fisher, Two-dimensional surface state in the quantum limit of a topological insulator, *Nature Physics* **6**, 960 (2010).

[11] T. Thio, S. Solin, J. Bennett, D. Hines, M. Kawano, N. Oda, and M. Sano, Giant magnetoresistance in zero-band-gap hg 1- x cd x te, *Physical Review B* **57**, 12239 (1998).

[12] N. P. Butch, K. Kirshenbaum, P. Syers, A. B. Sushkov, G. S. Jenkins, H. D. Drew, and J. Paglione, Strong surface scattering in ultrahigh-mobility bi₂ se₃ topological insulator crystals, *Physical Review B* **81**, 241301 (2010).

[13] S. Jia, H. Ji, E. Climent-Pascual, M. Fuccillo,

M. Charles, J. Xiong, N. P. Ong, and R. J. Cava, Low-carrier-concentration crystals of the topological insulator bi 2 te 2 se, *Physical Review B* **84**, 235206 (2011).

[14] Y.-q. Li, K.-h. Wu, J.-r. Shi, and X.-c. Xie, Electron transport properties of three-dimensional topological insulators, *Frontiers of Physics* **7**, 165 (2012).

[15] A. Roth, C. Brüne, H. Buhmann, L. W. Molenkamp, J. Maciejko, X.-L. Qi, and S.-C. Zhang, Nonlocal transport in the quantum spin hall state, *Science* **325**, 294 (2009).

[16] C.-Z. Chang, W. Zhao, D. Y. Kim, P. Wei, J. K. Jain, C. Liu, M. H. Chan, and J. S. Moodera, Zero-field dissipationless chiral edge transport and the nature of dissipation in the quantum anomalous hall state, *Physical review letters* **115**, 057206 (2015).

[17] Y. Ando, T. Hamasaki, T. Kurokawa, K. Ichiba, F. Yang, M. Novak, S. Sasaki, K. Segawa, Y. Ando, and M. Shiraishi, Electrical detection of the spin polarization due to charge flow in the surface state of the topological insulator bi1. 5sb0. 5te1. 7se1. 3, *Nano letters* **14**, 6226 (2014).

[18] J. Tian, I. Miotkowski, S. Hong, and Y. P. Chen, Electrical injection and detection of spin-polarized currents in topological insulator bi2te2se, *Scientific reports* **5**, 14293 (2015).

[19] S. Souma, K. Kosaka, T. Sato, M. Komatsu, A. Takayama, T. Takahashi, M. Kriener, K. Segawa, and Y. Ando, Direct measurement of the out-of-plane spin texture in the dirac-cone surface state of a topological insulator, *Physical review letters* **106**, 216803 (2011).

[20] Z.-H. Pan, E. Vescovo, A. Fedorov, D. Gardner, Y. Lee, S. Chu, G. Gu, and T. Valla, Electronic structure of the topological insulator bi 2 se 3 using angle-resolved photoemission spectroscopy: evidence for a nearly full surface spin polarization, *Physical review letters* **106**, 257004 (2011).

[21] D. Hsieh, Y. Xia, L. Wray, D. Qian, A. Pal, J. Dil, J. Osterwalder, F. Meier, G. Bihlmayer, C. Kane, *et al.*, Observation of unconventional quantum spin textures in topological insulators, *Science* **323**, 919 (2009).

[22] M. He, H. Sun, and Q. L. He, Topological insulator: Spintronics and quantum computations, *Frontiers of Physics* **14**, 1 (2019).

[23] Y. Fan and K. L. Wang, Spintronics based on topological insulators, in *Spin*, Vol. 6 (World Scientific, 2016) p. 1640001.

[24] Q. L. He, T. L. Hughes, N. P. Armitage, Y. Tokura, and K. L. Wang, Topological spintronics and magnetoelectronics, *Nature materials* **21**, 15 (2022).

[25] T. Yokoyama and S. Murakami, Spintronics and spin caloritronics in topological insulators, *Physica E: Low-dimensional Systems and Nanostructures* **55**, 1 (2014).

[26] H. P. Paudel and M. N. Leuenberger, Three-dimensional topological insulator quantum dot for optically controlled quantum memory and quantum computing, *Physical Review B* **88**, 085316 (2013).

[27] G. Scappucci, P. Taylor, J. Williams, T. Ginley, and S. Law, Crystalline materials for quantum computing: Semiconductor heterostructures and topological insulators exemplars, *MRS Bulletin* **46**, 596 (2021).

[28] N. Xu, Y. Xu, and J. Zhu, Topological insulators for thermoelectrics, *npj Quantum Materials* **2**, 51 (2017).

[29] Y. V. Ivanov, A. T. Burkov, and D. A. Pshenay-

- Severin, Thermoelectric properties of topological insulators, *physica status solidi (b)* **255**, 1800020 (2018).
- [30] S. Y. Matsushita, K. K. Huynh, H. Yoshino, N. H. Tu, Y. Tanabe, and K. Tanigaki, Thermoelectric properties of 3d topological insulator: Direct observation of topological surface and its gap opened states, *Physical Review Materials* **1**, 054202 (2017).
- [31] L. Muechler, F. Casper, B. Yan, S. Chadov, and C. Felser, Topological insulators and thermoelectric materials (2013).
- [32] Y. Xu, Thermoelectric effects and topological insulators, *Chinese Physics B* **25**, 117309 (2016).
- [33] G. Li and C. Felser, Heterogeneous catalysis at the surface of topological materials, *Applied Physics Letters* **116**, 070501 (2020).
- [34] L. Muechler, Topological classification of molecules and chemical reactions with a perplectic structure, *Physical Review B* **101**, 045123 (2020).
- [35] P. Narang, C. A. Garcia, and C. Felser, The topology of electronic band structures, *Nature Materials* **20**, 293 (2021).
- [36] L. M. Schoop, F. Pielnhofer, and B. V. Lotsch, Chemical principles of topological semimetals, *Chemistry of Materials* **30**, 3155 (2018).
- [37] G. Weng, W. Laderer, and A. N. Alexandrova, Understanding the adiabatic evolution of surface states in tetradymite topological insulators under electrochemical conditions, *The Journal of Physical Chemistry Letters* (2024).
- [38] Y. Rouzhahong, M. Wushuer, M. Mamat, Q. Wang, and Q. Wang, First principles calculation for photocatalytic activity of gaas monolayer, *Scientific reports* **10**, 9597 (2020).
- [39] X. Lv, W. Wei, Q. Sun, F. Li, B. Huang, and Y. Dai, Two-dimensional germanium monochalcogenides for photocatalytic water splitting with high carrier mobility, *Applied Catalysis B: Environmental* **217**, 275 (2017).
- [40] X. Zhang, X. Zhao, D. Wu, Y. Jing, and Z. Zhou, Mnpse3 monolayer: A promising 2d visible-light photohydrolytic catalyst with high carrier mobility, *Advanced science* **3**, 1600062 (2016).
- [41] C. R. Rajamathi, U. Gupta, N. Kumar, H. Yang, Y. Sun, V. Süß, C. Shekhar, M. Schmidt, H. Blumtritt, P. Werner, *et al.*, Weyl semimetals as hydrogen evolution catalysts, *Advanced Materials* **29**, 1606202 (2017).
- [42] G. Li, Q. Xu, W. Shi, C. Fu, L. Jiao, M. E. Kamminga, M. Yu, H. Tüysüz, N. Kumar, V. Süß, *et al.*, Surface states in bulk single crystal of topological semimetal co3sn2s2 toward water oxidation, *Science Advances* **5**, eaaw9867 (2019).
- [43] Y. He, D. Yan, L. R. Ng, L. Shi, S. Wang, H. Lin, S.-H. Lin, H. Luo, and K. Yan, Topological metal and non-centrosymmetric superconductor α -bipd as an efficient candidate for the hydrogen evolution reaction, *Materials Chemistry Frontiers* **3**, 2184 (2019).
- [44] S. Chen, Y.-M. Fang, J. Li, J.-J. Sun, G.-N. Chen, and H.-H. Yang, Study on the electrochemical catalytic properties of the topological insulator bi2se3, *Biosensors and Bioelectronics* **46**, 171 (2013).
- [45] C. Yang, M. Cattelan, N. Fox, Y. Huang, M. S. Golden, and W. Schwarzhacher, Electrochemical modification and characterization of topological insulator single crystals, *Langmuir* **35**, 2983 (2019).
- [46] J. Li, H. Ma, Q. Xie, S. Feng, S. Ullah, R. Li, J. Dong, D. Li, Y. Li, and X.-Q. Chen, Topological quantum catalyst: Dirac nodal line states and a potential electrocatalyst of hydrogen evolution in the TiSi family, *Science China Materials* **61**, 23 (2017).
- [47] H. Chen, W. Zhu, D. Xiao, and Z. Zhang, Co oxidation facilitated by robust surface states on au-covered topological insulators, *Physical review letters* **107**, 056804 (2011).
- [48] R. Hoffmann, A chemical and theoretical way to look at bonding on surfaces, *Reviews of modern Physics* **60**, 601 (1988).
- [49] B. Jiang and H. Guo, Dynamics in reactions on metal surfaces: A theoretical perspective, *The Journal of Chemical Physics* **150**, 180901 (2019).
- [50] G. Ertl, Elementary steps in heterogeneous catalysis, *Angewandte Chemie International Edition in English* **29**, 1219 (1990).
- [51] C. R. Second, E. Edition, G. Ertl, H. Knözinger, F. Schüth, J. Weitkamp, and W.-V. V. G. C. KGaA, Handbook of heterogeneous catalysis (2008).
- [52] V. May and O. Kühn, *Charge and energy transfer dynamics in molecular systems* (John Wiley & Sons, 2023).
- [53] A. M. Wodtke, D. Matsiev, and D. J. Auerbach, Energy transfer and chemical dynamics at solid surfaces: The special role of charge transfer, *Progress in surface science* **83**, 167 (2008).
- [54] N. S. Lewis, Chemical control of charge transfer and recombination at semiconductor photoelectrode surfaces, *Inorganic chemistry* **44**, 6900 (2005).
- [55] P. Weisz, Effects of electronic charge transfer between adsorbate and solid on chemisorption and catalysis, *The Journal of Chemical Physics* **21**, 1531 (1953).
- [56] R. A. Santen, *Theoretical heterogeneous catalysis*, Vol. 5 (World Scientific, 1991).
- [57] J. Jung, S. Kang, L. Nicolai, J. Hong, J. Minár, I. Song, W. Kyung, S. Cho, B. Kim, J. D. Denlinger, *et al.*, Understanding the role of electronic effects in co on the pt-sn alloy surface via band structure measurements, *ACS Catalysis* **12**, 219 (2021).
- [58] K. McKenna, T. Trevethan, and A. Shluger, Interplay between adsorbate diffusion and electron tunneling at an insulating surface, *Physical Review B* **82**, 085427 (2010).
- [59] E. Wahlstrom, E. K. Vestergaard, R. Schaub, A. Rønnau, M. Vestergaard, E. Lægsgaard, I. Stensgaard, and F. Besenbacher, Electron transfer-induced dynamics of oxygen molecules on the tio2 (110) surface, *Science* **303**, 511 (2004).
- [60] B. Kasemo, Charge transfer, electronic quantum processes, and dissociation dynamics in molecule-surface collisions, *Surface science* **363**, 22 (1996).
- [61] H.-L. Dai and W. Ho, *Laser Spectroscopy and Photochemistry on Metal Surfaces* (World Scientific Publishing Company, 1995).
- [62] B. Persson and M. Persson, Vibrational lifetime for co adsorbed on cu (100), *Solid State Communications* **36**, 175 (1980).
- [63] P. W. Anderson, Localized magnetic states in metals, *Physical Review* **124**, 41 (1961).
- [64] D. Newns, Self-consistent model of hydrogen chemisorption, *Physical Review* **178**, 1123 (1969).
- [65] J. C. Tully, Molecular dynamics with electronic transi-

- tions, *The Journal of Chemical Physics* **93**, 1061 (1990).
- [66] M. Head-Gordon and J. C. Tully, Molecular dynamics with electronic frictions, *The Journal of Chemical Physics* **103**, 10137 (1995).
- [67] J. C. Tully, Chemical dynamics at metal surfaces, *Annual Review of Physical Chemistry* **51**, 153 (2000).
- [68] A. M. Wodtke, J. C. Tully, and D. J. Auerbach, Electronically non-adiabatic interactions of molecules at metal surfaces: Can we trust the born-oppenheimer approximation for surface chemistry?, *International Reviews in Physical Chemistry* **23**, 513 (2004).
- [69] B. Hellsing and M. Persson, Electronic damping of atomic and molecular vibrations at metal surfaces, *Physica Scripta* **29**, 360 (1984).
- [70] S. Ghan, E. Diesen, C. Kunkel, K. Reuter, and H. Oberhofer, Interpreting ultrafast electron transfer on surfaces with a converged first-principles newns-anderson chemisorption function, *The Journal of Chemical Physics* **158** (2023).
- [71] M. Persson and B. Hellsing, Electronic damping of adsorbate vibrations on metal surfaces, *Physical Review Letters* **49**, 662 (1982).
- [72] J. Juaristi, M. Alducin, R. D. Muiño, H. F. Busnengo, and A. Salin, Role of electron-hole pair excitations in the dissociative adsorption of diatomic molecules on metal surfaces, *Physical review letters* **100**, 116102 (2008).
- [73] D.-H. Nam, P. De Luna, A. Rosas-Hernández, A. Thevenon, F. Li, T. Agapie, J. C. Peters, O. Shekhah, M. Eddaoudi, and E. H. Sargent, Molecular enhancement of heterogeneous co₂ reduction, *Nature materials* **19**, 266 (2020).
- [74] J. Schneider, H. Jia, J. T. Muckerman, and E. Fujita, Thermodynamics and kinetics of co₂, co, and h+ binding to the metal centre of co₂ reduction catalysts, *Chemical Society Reviews* **41**, 2036 (2012).
- [75] C. S. Diercks, Y. Liu, K. E. Cordova, and O. M. Yaghi, The role of reticular chemistry in the design of co₂ reduction catalysts, *Nature materials* **17**, 301 (2018).
- [76] A. Ge, B. Rudsteyn, J. Zhu, R. J. Maurer, V. S. Batista, and T. Lian, Electron-hole-pair-induced vibrational energy relaxation of rhenium catalysts on gold surfaces, *The Journal of Physical Chemistry Letters* **9**, 406 (2018).
- [77] K. L. Materna, R. H. Crabtree, and G. W. Brudvig, Anchoring groups for photocatalytic water oxidation on metal oxide surfaces, *Chemical Society Reviews* **46**, 6099 (2017).
- [78] W. P. Su, J. R. Schrieffer, and A. J. Heeger, Solitons in polyacetylene, *Phys. Rev. Lett.* **42**, 1698 (1979).
- [79] A. J. Heeger, S. Kivelson, J. R. Schrieffer, and W. P. Su, Solitons in conducting polymers, *Rev. Mod. Phys.* **60**, 781 (1988).
- [80] A.-M. Visuri, C. Berthod, and T. Giamarchi, Impurity coupled to a lattice with disorder, *Physical Review A* **98**, 053607 (2018).
- [81] W.-P. Su, J. Schrieffer, and A. Heeger, Soliton excitations in polyacetylene, *Physical Review B* **22**, 2099 (1980).
- [82] U. Fano, Effects of configuration interaction on intensities and phase shifts, *Physical review* **124**, 1866 (1961).
- [83] H. Takayama, Y. R. Lin-Liu, and K. Maki, Continuum model for solitons in polyacetylene, *Physical Review B* **21**, 2388 (1980).
- [84] M. Suzuki and K. Nasu, Dynamics of charge transfer from molecule to semiconductor at surface: Numerical method for nonadiabaticity and irreversibility in discrete-continuum transition, *The Journal of Chemical Physics* **92**, 4576 (1990).
- [85] S. Masato, Dynamics of electron-hole pair creation at semiconductor surface via charge transfer between molecule and solid, *The Journal of Chemical Physics* **105**, 1584 (1996).
- [86] S. Saini, J. Halldin Stenlid, and F. Abild-Pedersen, Electronic structure factors and the importance of adsorbate effects in chemisorption on surface alloys, *npj Computational Materials* **8**, 163 (2022).
- [87] A. A. Dzhiboev, D. S. Kosov, and F. Von Oppen, Out-of-equilibrium catalysis of chemical reactions by electronic tunnel currents, *The Journal of Chemical Physics* **138**, 134103 (2013).
- [88] W. Dou and J. E. Subotnik, Perspective: How to understand electronic friction, *Journal of Chemical Physics* **148** (2018).
- [89] W. Dou and J. E. Subotnik, Nonadiabatic molecular dynamics at metal surfaces, *The Journal of Physical Chemistry A* **124**, 757 (2020).
- [90] H. Spohn, Kinetic equations from hamiltonian dynamics: Markovian limits, *Reviews of Modern Physics* **52**, 569 (1980).
- [91] R. Dann, A. Levy, and R. Kosloff, Time-dependent markovian quantum master equation, *Physical Review A* **98**, 052129 (2018).
- [92] I. G. Ryabinkin and A. F. Izmaylov, Mixed quantum-classical dynamics using collective electronic variables: A better alternative to electronic friction theories, *The Journal of Physical Chemistry Letters* **8**, 440 (2017).
- [93] Y. Huang, C. T. Rettner, D. J. Auerbach, and A. M. Wodtke, Vibrational promotion of electron transfer, *Science* **290**, 111 (2000).
- [94] O. Bünermann, H. Jiang, Y. Dorenkamp, A. Kandratsenka, S. M. Janke, D. J. Auerbach, and A. M. Wodtke, Electron-hole pair excitation determines the mechanism of hydrogen atom adsorption, *Science* **350**, 1346 (2015).
- [95] R. J. Maurer, M. Askerka, V. S. Batista, and J. C. Tully, Ab initio tensorial electronic friction for molecules on metal surfaces: Nonadiabatic vibrational relaxation, *Physical Review B* **94**, 115432 (2016).
- [96] G. Kresse and J. Furthmüller, Efficiency of ab-initio total energy calculations for metals and semiconductors using a plane-wave basis set, *Computational materials science* **6**, 15 (1996).
- [97] N. W. Ashcroft and N. D. Mermin, *Solid state physics* (Cengage Learning, 2022).
- [98] J. Sjakste, N. Vast, G. Barbarino, M. Calandra, F. Mauri, J. Kanasaki, H. Tanimura, and K. Tanimura, Energy relaxation mechanism of hot-electron ensembles in gaas: Theoretical and experimental study of its temperature dependence, *Physical Review B* **97**, 064302 (2018).
- [99] F. Giustino, Electron-phonon interactions from first principles, *Reviews of Modern Physics* **89**, 015003 (2017).
- [100] B. Burrows and A. Amos, Wide-band approximation in the theories of charge transfer during ion-surface scattering, *Physical Review B* **49**, 5182 (1994).